

Transformable optical dipole trap using a phase-modulated standing wave

Seung Koo Lee, Jae Jin Kim, and D. Cho*

Department of Physics, Korea University, Seoul 136-713, Korea

(Received 17 August 2006; published 4 December 2006)

We demonstrate a new type of a cavity-enhanced optical trap whose standing-wave potential well can be transformed by using phase modulation. When the modulation frequency is matched to the free spectral range of the cavity, the potential well can be changed continuously from a corrugated form of a standing wave to a flattened form of a traveling wave depending on the modulation index. With the phase modulation, more atoms are trapped due to the increase in the trap volume, and there is a pronounced increase by a factor of 1.9 when an optimal modulation is applied. From the increase in number of trapped atoms we also infer that the temperature associated with longitudinal motion is strongly affected by the transformation of the potential well. This technique can be used to study collective behavior of trapped atoms and to manipulate atomic distribution for quantum information processing.

DOI: [10.1103/PhysRevA.74.063401](https://doi.org/10.1103/PhysRevA.74.063401)

PACS number(s): 32.80.Pj, 07.60.Ly

I. INTRODUCTION

Optical trapping of neutral atoms has evolved into many different forms and continues to find new and exciting applications. An optical dipole trap was employed to create Bose Einstein condensates (BEC) of both rubidium [1] and cesium atoms [2]. Optically trapped strontium [3] or ytterbium atoms [4] are intensively studied as candidates for the next-generation frequency standard based on the frequency comb technique.

As first demonstrated in 1993 [5], it is advantageous to use a laser beam with high power and large detuning in order to trap many atoms with minimum perturbation. Such a trap is called a far-off-resonance optical trap (FORT). One manifestation of a FORT with extreme detuning and power is a quasioleostatic trap produced by a CO₂ laser [6]. Such a trap is used to create the rubidium and cesium BEC. Another approach is to employ an optical resonator as a power buildup cavity (PBC). Both a ring cavity [7] and a Fabry-Perot cavity [8,9] were used to increase the intracavity power by two or three orders of magnitude. In addition to the power enhancement, a cavity with its boundary condition produces discrete resonant modes. Interaction between the modes and the trapped atoms presents many interesting phenomena. For example, a new cooling mechanism for atoms inside a cavity stimulated by the cavity modes was discovered [10]. Conversely, optically trapped atoms can change the cavity resonance frequency. By manipulating the dispersive property of the atoms one may be able to construct a device like an optical transistor. The standing wave formed inside a Fabry-Perot cavity traps atoms at equally spaced antinodes, thereby producing an optical lattice [11].

In this paper we report a new type of a cavity-enhanced FORT whose standing-wave potential well can be transformed by using a phase modulation technique. When the modulation frequency is matched to the free spectral range, both carrier and sidebands of the input beam can couple to the cavity. By adjusting the modulation index, the intensity

distribution near the center of the cavity can be continuously changed from a corrugated form of a standing wave to a flattened form of a traveling wave. Such a capability provides many interesting experimental possibilities: (i) Dynamic control of the modulation index can lead to adiabatic cooling (or heating) of longitudinal motion of trapped atoms. The cooling factor is the ratio of the oscillation frequency for atoms confined in a standing wave to that in a Gaussian beam. In harmonic approximation it is $2\pi z_0/\lambda$, where z_0 is the Rayleigh range and λ is the wavelength. For our experimental parameters, it is 5.6×10^4 . The cooling is effective only for the longitudinal degree of freedom and due to the Liouville theorem such a cooling mechanism cannot increase the phase space density. As in the cesium BEC experiment [2], however, with proper addition of trapping beams it can be used as a step toward an optical BEC. (ii) The standing wave inside a Fabry-Perot cavity forms an optical lattice. The height of the potential barrier can be controlled by changing the modulation index. Recently, BEC atoms transferred to an optical lattice have opened new research in condensed matter physics [12] and quantum information processing [13]. The group at NIST developed a superlattice constructed by two commensurate standing waves to load BEC atoms in every third site of a one-dimensional optical lattice [14]. The group at Max Planck Institute developed a technique to transform an optical lattice by changing polarization of the counterpropagating laser beams [15]. Our method of phase modulation can add another technique to the tool box for quantum information processing. (iii) The phase shift between the transmitted carrier and sidebands can be used as a sensitive measure of the dispersive property of trapped atoms in a manner similar to the Pound-Drever-Hall [16] method which uses the phase shift of the reflected beams as a measure of frequency offset. The group at JILA improved the sensitivity of FM spectroscopy dramatically by using a cavity-enhanced FM spectroscopy, where both carrier and sidebands are resonant with the cavity [17]. (iv) It is sometimes useful to have both smooth intensity distribution and power enhancement without having to use a ring cavity. For optical trapping, a traveling-wave-like distribution gives larger trap volume than that of a standing wave. In the experiment to measure the parity nonconservation from atomic

*e-mail address: cho@korea.ac.kr

cesium [18], a Fabry-Perot cavity was used as a PBC to drive a very weak $6S$ - $7S$ transition. A large intensity gradient of the standing wave was a source of one of the systematic effects [19], and the situation could have been ameliorated by using the phase modulation technique [20].

II. THEORY

When an oscillating electric field $E_m \sin \omega_m t$ is applied to an electro-optic crystal like lithium niobate (LiNbO_3), the index of refraction of the crystal is modulated by $\Delta n \sin \omega_m t$. As a laser beam with a polarization along the optic axis passes through the crystal of length l , its field is phase modulated due to the index modulation. The electric field of the output beam can be written as $E_{\text{out}}(z, t) = E_0 e^{i(k_0 z - \omega_0 t + \alpha \sin(\omega_m t - k_m z))}$, where $k_0 = \omega_0/c$ is the wave vector in vacuum, $k_m = \omega_m/c$ is the change in the wave vector corresponding to the frequency change by ω_m . $\alpha = \Delta n k_0 l$ is the modulation index. From the Jacobi-Anger relation, the output field can be expanded in terms of a carrier and sidebands,

$$E_{\text{out}}(z, t) = E_0 e^{i(k_0 z - \omega_0 t)} \{ J_0(\alpha) + J_1(\alpha) e^{i(\omega_m t - k_m z)} - J_1(\alpha) e^{-i(\omega_m t - k_m z)} + \dots \}, \quad (1)$$

where J 's are Bessel functions.

When the carrier is resonant with the n th mode of a Fabry-Perot cavity of length L ($\omega_0 = 2\pi \times nc/2L$) and the modulation frequency ω_m is set to be the same as the free spectral range (FSR) of the cavity, $2\pi \times c/2L$, the carrier and all the sidebands can simultaneously couple to the cavity. Each frequency component forms a standing wave inside the cavity. Considering up to the first-order sidebands, the intracavity on-axis intensity distribution over $0 \leq z \leq L$ is given by

$$I(z) = I_0 \{ J_0^2(\alpha) \sin^2 k_0 z + J_1^2(\alpha) \sin^2(k_0 + k_m)z + J_1^2(\alpha) \times \sin^2(k_0 - k_m)z \}, \quad (2)$$

where we neglect interference among the carrier and the sidebands. The interference terms oscillate at either ω_m or its integer multiples. In our apparatus $L = 4.15$ cm, and $\omega_m = 2\pi \times 3.61$ GHz. The frequency is too high for an atom to follow and it is far away from any of the internal atomic resonances. We note that the real intracavity field is Gaussian with its focus at the center and the intensity distribution in Eq. (2) should be multiplied by the Gaussian envelope factor, $1 + (z - L/2)^2/z_0^2$.

If n for the carrier mode is odd, the standing wave has an antinode at the cavity center. See Fig. 1(a) for $n = 11$. The first-order sidebands correspond to the $(n \pm 1)$ th modes. The intensity profile of the twelfth mode is shown in Fig. 1(b). Because the even-ordered mode has a node at the cavity center, the intensity distribution near the center becomes flattened when both the carrier and the sidebands are present. Especially when $\alpha = 1.2$, $J_0^2(\alpha) = 2J_1^2(\alpha)$ and the intracavity power is evenly distributed between the carrier and the first-order sidebands. In this case, the intensity profile near $z = L/2$ becomes flat as shown in Fig. 1(c). As one moves away from the cavity center, corrugation grows due to the

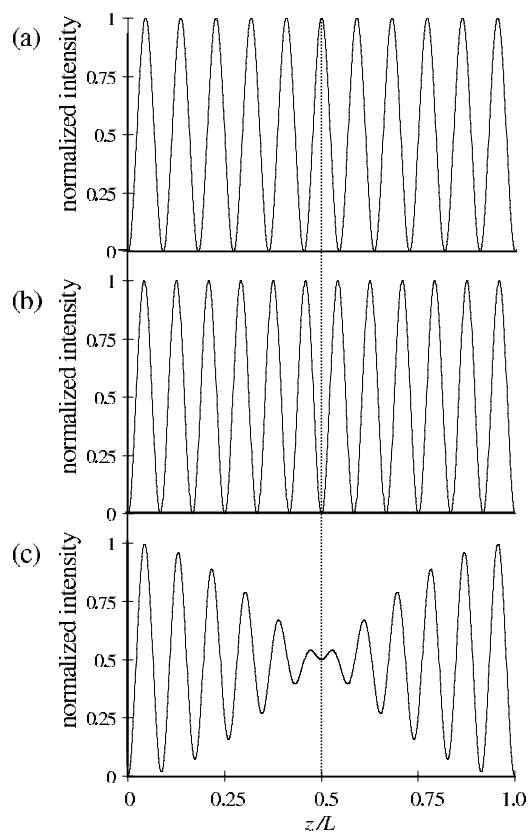


FIG. 1. Intracavity on-axis intensity distributions of (a) carrier with $n = 11$, (b) first-order sideband with $n = 12$, and (c) sum of the carrier and the sidebands when the modulation index is 1.2. In this figure we neglect the Gaussian envelope factor.

accumulated phase mismatch between the carrier and the sidebands. In the figures we use $n \approx 10$ and the corrugation becomes apparent within half a wavelength. For the Fabry-Perot cavity used in the experiment $n \approx 10^5$ and the region with local maximum intensity smaller than 10% of the average intensity extends over ± 3 mm.

III. APPARATUS

Our experimental apparatus consists of two vacuum chambers, a cubic chamber for a low velocity intense source (LVIS) [21] and an octagonal chamber for an optical dipole trap. The experimental apparatus is shown in Fig. 2 and it was described in detail in [9]. The PBC placed diagonally inside the octagonal chamber consists of two identical 2.5-cm radius-of-curvature mirrors, which are separated by 4.15 cm. The minimum spot size at the center for the Gaussian mode is $48 \mu\text{m}$. At the design wavelength of 895 nm, each mirror has 0.35% transmission and the full width at half-maximum of the cavity resonance is 4.0 MHz. The intensity at the antinode of the intracavity standing wave is 1100 times the peak intensity of the input Gaussian beam. Because once the chamber is sealed and evacuated we cannot readjust the cavity alignment anymore, much care was taken in designing mirror mounts [22]. We use a single-mode Ti:sapphire laser as a light source for the FORT beam. We

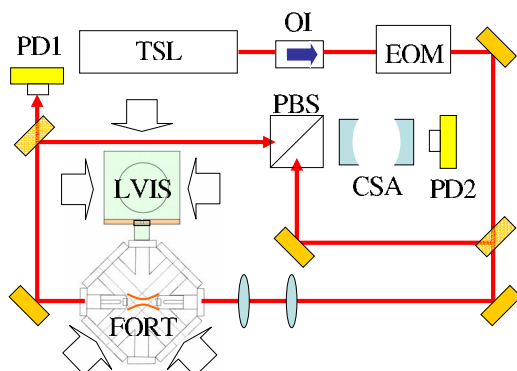


FIG. 2. (Color online) Experimental apparatus. TSL: Ti:sapphire laser, OI: optical isolator, EOM: electro-optic modulator, PBS: polarizing beam splitter, CSA: confocal spectrum analyzer, LVIS: low velocity intense source, FORT: far-off-resonance optical trap, and PD1 and PD2: photo-detectors for the PBC and CSA transmissions, respectively. Vertical beams for the LVIS and the second MOT are not shown.

developed systems that control all aspects of the laser beam, namely mode matching and frequency locking/relocking to the cavity, power stabilization, as well as polarization control. Details of the frequency control are given in [23].

A slow atomic beam is produced by the LVIS constructed around the cubic chamber. The slow beam is used to load another magneto-optical trap (MOT), which we call a second MOT, formed at the center of the octagonal chamber [24]. The pressure in the octagon is 1.3×10^{-9} Torr. Trapping beams for the LVIS and the MOT are provided by two 60-mW slave lasers injection-locked by a single master laser. Spatial mode of the trapping beam affected MOT shape and its overlap with the FORT beam. The trapping beam for the second MOT is spatially filtered by a $15\text{-}\mu\text{m}$ pinhole and the mode-filtered power is 30 mW. Another extended-cavity diode laser is used to provide hyperfine repumping for both the LVIS and the second MOT. We use a dark-spot MOT to maximize transfer efficiency from the second MOT to the FORT. A 5-mm diameter dark spot on the repumping beam is imaged at the center of the octagon by a 2-m long telescope. In order to measure the number of trapped atoms, fluorescence from the atomic cloud is imaged onto a photodiode. We also have a setup for absorption imaging to measure the spatial distribution and temperature of the optically trapped atoms.

A new feature of the apparatus is a phase modulation system shown in Fig. 3 based on a microwave electro-optic modulator (EOM). We use a YIG (yttrium iron garnet) oscillator (Micro Lambda Model MLOS-0104A) to provide 3.61-GHz microwaves to the EOM (New Focus Model 4431). Because the modulation frequency should match the FSR of the cavity within a small fraction of the 4.0-MHz cavity linewidth, we installed a digital servo system that could keep the YIG frequency stable to within 10 kHz. A computer monitors frequency drift using a stable frequency counter and an analog output from the computer controls a precision current supply to fine tune the YIG oscillator. Output power of 40 mW from the YIG oscillator goes through a circulator (Nova Microwave Model 0380CES), which protects the os-

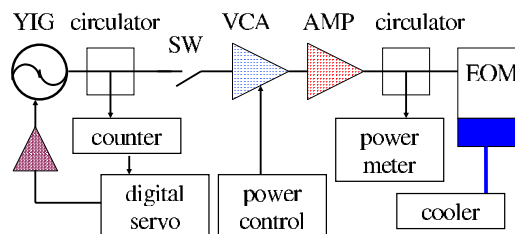


FIG. 3. (Color online) Phase modulation system. YIG: yttrium iron garnet tuned oscillator, SW: TTL-controlled microwave switch, VCA: voltage-controlled attenuator, and AMP: power amplifier.

cillator and directs reflected power to the frequency counter. A TTL-controlled switch (Universal Microwave Components Corp. Model SR-S010-15) and a voltage-controlled attenuator (Universal Microwave Components Corp. Model AT-H000-HV) controls power. Finally, a power amplifier drives the EOM. The custom-made amplifier (Microwave Amplifiers Ltd. Model 38-3.5S) has a fixed gain of 30 dB near 3.6 GHz and puts out up to 5 W. The EOM crystal is placed in a microwave resonant cavity and its cavity linewidth is only 1 MHz. At resonance the EOM is a $50\text{-}\Omega$ load, but off resonance it reflects much of the applied microwave power. A circulator and an isolator (not shown in the figure) are added between the amplifier and the EOM to monitor the reflected power as well as to protect the amplifier. The EOM resonant cavity can be tuned over 100 MHz near 3.6 GHz using a tuning fork.

In order to reach the target modulation index of 1.2, approximately 2.5 W of microwave power should be applied to the EOM. Such a high-power operation causes a few problems. First is a thermal drift of the EOM resonance frequency and subsequent reflection of the microwave power. Second, a thermal lensing effect from inhomogeneous warming of the EOM crystal and subsequent steering of the laser beam can result. To reduce these thermal effects, we cooled the EOM down to $0\text{ }^\circ\text{C}$ using both thermoelectric coolers and a water cooling system. We placed the EOM and the cooling system in a vacuum can to avoid water condensation on the EOM windows. With the cooling, the thermal drift is reduced enough to allow stable production of the sidebands, and the thermal lensing is also substantially reduced. As α approaches 1.2, however, the FORT beam is still steered off the input mirror of the Fabry-Perot cavity, which is placed 2 m downstream from the EOM. Fortunately, the thermal lensing effect only steers the beam without degrading its Gaussian mode. We can restore most of the power buildup by simply realigning the beam. The need for a realignment, however, means that dynamic control of the modulation index is not possible with our current setup.

IV. EXPERIMENT AND RESULTS

Each measurement cycle begins by loading the second dark-spot MOT from the LVIS beam for 3 s. The FORT beam either with or without the phase modulation stays on while the MOT is loaded. At the end of the MOT loading period, we close shutters for the LVIS light and there is an optional FORT loading stage of 50 ms during which the re-

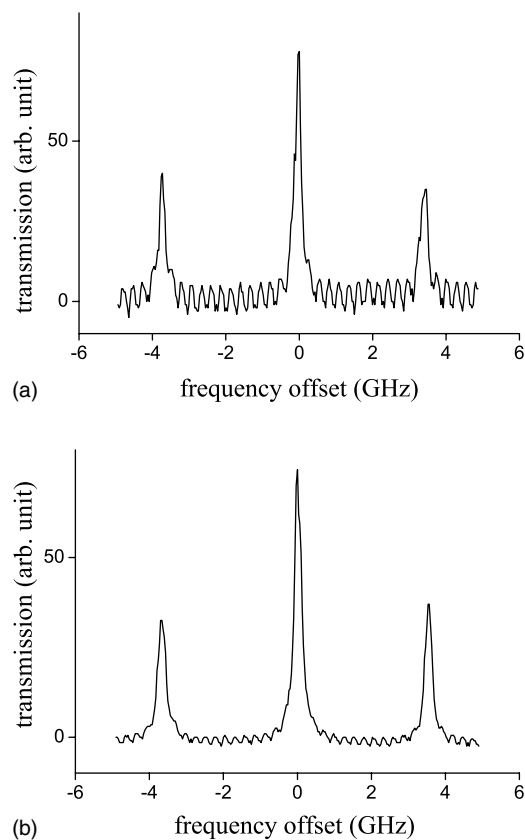


FIG. 4. Spectrum of a phase-modulated laser beam (a) after the EOM and (b) after the PBC. The small features are from 60-Hz noise.

pumping power and trapping power and detuning can be changed. It is followed by a FORT holding period of at least 200 ms during which the second MOT light is off and untrapped MOT atoms disperse away. Then we turn off the FORT beam and immediately turn back on the MOT light and integrate the imaged fluorescence for 220 ms to measure the number of atoms that stay trapped in the FORT. Because the LVIS is off, virtually no atoms are added to the second MOT during this fluorescence measurement. Finally, there is a 160-ms MOT-off time followed by another 220-ms MOT fluorescence measurement to find background offset due to light scattering. The next measurement cycle is initiated as soon as the Ti:sapphire laser frequency is locked to the cavity by an automatic relock system. For a typical FORT loading experiment, we use a FORT beam wavelength of 895 nm. The maximum power transmitted from the cavity is 90 mW, which implies that at the antinode the intensity is 2.9 MW/cm² and the well depth is 9.0 mK. A FORT loading experiment without a phase modulation is described in our previous publication [9].

In order to add the phase modulation we first align the polarization of the FORT beam vertically along the optic axis of the LiNbO₃ crystal by rotating the optical isolator. An upstream half-waveplate controls the laser power transmitted through the isolator. We measure the fractional size of the sidebands and thereby the modulation index using a confocal spectrum analyzer with 3.0-GHz FSR. See Fig. 2. Figure 4(a) shows the spectrum of the beam after the EOM when 2.5 W

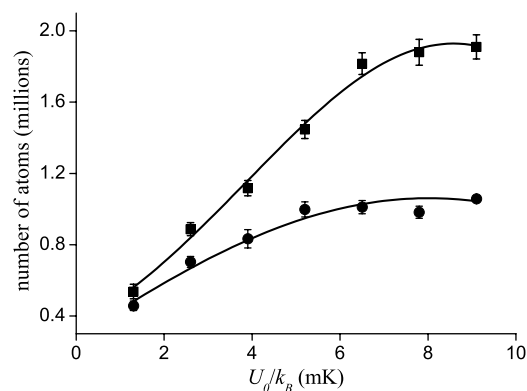


FIG. 5. Number of optically trapped atoms without phase modulation (lower curve) and with an optimal phase modulation (upper curve).

of microwave power is applied. The EOM resonance frequency is tuned by minimizing the reflected power. The size of the first-order sideband is approximately half of the carrier, and the spectrum is symmetric with respect to the carrier. Next, we lock the laser frequency to the PBC and measure the spectrum of the transmitted beam by directing it to the same confocal spectrum analyzer through a polarizing beam splitter. When the modulation frequency is the same as the FSR of the PBC, the fractional size of the first-order sidebands on the upstream and downstream sides of the PBC should be the same. See Fig. 4(b). More sensitive measure of the frequency matching, however, is the asymmetry between the plus and the minus first-order sidebands of the downstream beam as the carrier frequency is slightly detuned from the cavity resonance. We use this technique by locking the carrier frequency to either side of the PBC resonance and find that the FSR of the PBC is 3.6114 GHz.

Curves in Fig. 5 show the number of atoms trapped in the FORT while the well depth U_0 is changed. The lower curve is without the phase modulation and the upper one is when the modulation index is 1.2. Each pair of data points at the same U_0 are taken with the power transmitted through the cavity kept constant. U_0 is defined as the peak well depth at an antinode of the standing wave without phase modulation for a given PBC-transmitted power. When $\alpha=1.2$, the actual well depth of the flattened potential is half of U_0 . From the data we first note that the number N of trapped atoms tends to saturate after $U_0/k_B=6$ mK. In an optical trap N is limited by the atom number density, or equivalently by the effective trap volume. As long as the ratio of the temperature of trapped atoms to the local well depth is constant, the trap volume does not increase with the deeper well. From the temperature measurement using absorption imaging we find that the ratio $k_B T/U_0$ is constant at ~ 0.4 . Second, we note that there is a factor of 1.9 increase in N when the optimal phase modulation is applied for U_0/k_B larger than 5 mK. This can be explained by the increase in the trap volume. The potential well of a phase-modulated standing wave near the cavity center can be written in cylindrical coordinate as

$$U(\rho, z) = -U_0 e^{-2\rho^2/w_0^2} [\beta \cos^2 k_0 z + (1 - \beta) \sin^2 k_0 z], \quad (3)$$

where w_0 is the minimum spot size, and β is related to the modulation index by

$$\frac{1-\beta}{2\beta} = \left[\frac{J_1(\alpha)}{J_0(\alpha)} \right]^2. \quad (4)$$

$\beta=1$ corresponds to $\alpha=0$ and $\beta=0.5$ to $\alpha=1.2$. From the potential well we can calculate the effective trap volume over a half wavelength assuming a Maxwell-Boltzmann distribution:

$$v_{\text{eff}}(\beta) = \frac{\eta\pi w_0^2}{\beta} \cdot \frac{\left[\int_{-\lambda/4}^{\lambda/4} \exp\{Q(z, \beta)/\eta\} dz \right]^2}{\int_{-\lambda/4}^{\lambda/4} \exp\{2Q(z, \beta)/\eta\} dz}, \quad (5)$$

where $\eta = k_B T / U_0$ and $Q(z, \beta) = \beta \cos^2 k_0 z + (1-\beta) \sin^2 k_0 z$. For a transverse confinement, we use a harmonic approximation, $e^{-2\rho^2/w_0^2} \approx 1 - 2\rho^2/w_0^2$, and put $|U(0, 0)| = \beta U_0$ as the peak well depth. From the temperature measurement we find that as the peak well depth is reduced to βU_0 due to phase modulation, the temperature associated with transverse motion is also reduced by the same factor keeping the ratio $k_B T / \beta U_0$ constant at ~ 0.4 . As a consequence, the effective trap area associated with the Gaussian beam profile, $\eta\pi w_0^2 / \beta$, remains constant. For a longitudinal confinement, we carry out numerical integrations along z to find that the ratio, $v_{\text{eff}}(0.5) / v_{\text{eff}}(1)$, is 1.6. This ratio is 15% smaller than the measured value of 1.9 in Fig. 5. We note that the ratio 1.6 is from the increase in trap volume over a single antinode and if atoms spread more along z axis due to flattening, there may be further increase in trap volume. When atoms are first loaded to an optical trap, their spatial distribution is largely determined by that of the MOT atoms. However, unlike a standing wave optical trap, where loaded atoms are confined to each antinode, in a phase-modulated case atoms can spill over to both sides along z axis. Unfortunately, we cannot measure the elongation factor because immediately after the FORT loading period there is a large background from nearby MOT atoms. We can only take the image after 200-ms FORT holding time, and from that measurement we find that the image with the optimal phase modulation is almost twice longer than that without a phase modulation. This measurement supports our hypothesis of the increment by spill-over effect.

Next we measure N as the modulation index is increased while the PBC-transmitted power is kept constant at $U_0/k_B = 9$ mK. The ratio of $N(r)/N(0)$ is shown in Fig. 6, where $r = (1-\beta)/2\beta$ is the fraction of a single first-order sideband power to the carrier power. The experimental data (●) shows a pronounced peak at $r=0.5$, where the potential well is flat. As the microwave power applied to the EOM is further increased, sideband-dominated corrugation appears and N begins to decrease. When $r=0.6$, however, the second-order sideband, which has been neglected so far, has 13% of the carrier power. The potential well is less corrugated at $r=0.6$ than at $r=0.4$, and $N(0.6) > N(0.4)$. The theory curve (Δ) is from the second factor in Eq. (5) multiplied by the elongation factor. We assume that the elongation factor scales linearly with r and put it to be $1+0.3r$. The theory curve shows poor agreement with the data. Due to the elon-

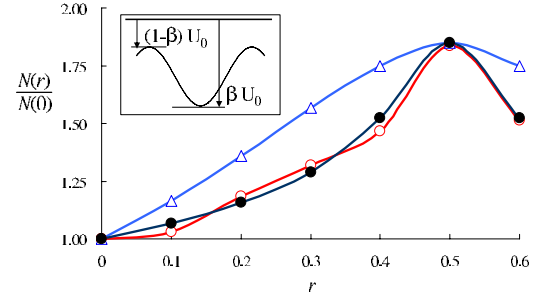


FIG. 6. (Color online) Fractional increase in the number of trapped atoms when the phase modulation is applied. r is the fraction of a single first-order sideband power to the carrier power. \circ : experimental data, Δ : theory curve when longitudinal temperature is assumed to be the same as the transverse temperature, and \bullet : theory curve with corrected longitudinal temperature. The inset shows the potential well along z axis with phase modulation.

gated shape of the atomic cloud we cannot measure the longitudinal temperature with enough precision, and for this calculation we simply assume that it is the same as the transverse temperature, $0.4\beta U_0/k_B$. As shown in the inset, however, the minimum well depth, from which the MOT atoms are transferred to the optical trap, is not 0, but $(1-\beta)U_0$. Because the temperature of optically trapped atoms is a fixed fraction (~ 0.4) of kinetic energy gained by MOT atoms during their fall into an optical potential well, we expect the longitudinal temperature lower than $0.4\beta U_0/k_B$. To take it into account, we define an effective well depth U_{eff} for the longitudinal degree of freedom as $\beta U_0 - q(1-\beta)U_0$, with $0 \leq q \leq 1$, and put the temperature to be $0.4U_{\text{eff}}/k_B$. We obtain best agreement with the data at $q=0.75$ as shown in the third curve (\circ). This analysis implies that the longitudinal temperature is substantially lower than the transverse temperature, leading to decrease in trap volume for $r < 0.5$. At $r=0.5$ the trap is flat and its effective length over an antinode is $\lambda/2$ independent of the temperature.

Finally, the lifetime of the atoms trapped in the FORT is measured by obtaining the number of atoms left in the FORT while increasing the FORT holding time from 200 ms to a few seconds at proper intervals. The lifetime is 450 ms regardless of the modulation index. The lifetime is largely limited by the collision with background molecules and it is not affected by the detailed shape of the potential wells.

V. SUMMARY AND DISCUSSION

We constructed an optical dipole trap using a PBC and developed a phase modulation technique to transform its potential well continuously from a corrugated form of a standing wave to a flattened form of a traveling wave. The number of trapped atoms increases by a factor of 1.9 due to the increase in trap volume. Dynamic application of the phase modulation can lead to adiabatic cooling and manipulation of trapped atoms for quantum information processing. Due to the thermal lensing problem, however, dynamic control was not demonstrated in this work. For dynamic control, we plan

to use a device for an automatic beam alignment to counteract the beam steering by the EOM. Alternatively we may use a solid etalon, whose transmission peaks coincide with the sidebands, so that smaller modulation index results in a flat potential well.

ACKNOWLEDGMENTS

This work was supported by the Korea Science and Engineering Foundation (R01-2005-10477) and by the Ministry of Education (2004-015-C00106). S.K.L. acknowledges support from the Seoul R&BD program.

-
- [1] M. Barrett, J. Sauer, and M. S. Chapman, *Phys. Rev. Lett.* **87**, 010404 (2001).
 - [2] T. Weber, J. Herbig, M. Mark, H. Nägerl, and R. Grimm, *Science* **299**, 232 (2003).
 - [3] M. Takamoto, F. Hong, R. Higashi, and H. Katori, *Nature (London)* **435**, 321 (2005); A. D. Ludlow, M. M. Boyd, T. Zelevinsky, S. M. Foreman, S. Blatt, M. Notcutt, T. Ido, and J. Ye, *Phys. Rev. Lett.* **96**, 033003 (2006).
 - [4] C. Y. Park and T. H. Yoon, *Phys. Rev. A* **68**, 055401 (2003); Z. W. Barber, C. W. Hoyt, C. W. Oates, L. Hollberg, A. V. Taichenachev, and V. I. Yudin, *Phys. Rev. Lett.* **96**, 083002 (2006).
 - [5] J. D. Miller, R. A. Cline, and D. J. Heinzen, *Phys. Rev. A* **47**, R4567 (1993).
 - [6] T. Takekoshi and R. J. Knize, *Opt. Lett.* **21**, 77 (1996).
 - [7] D. Kruse, M. Ruder, J. Benhelm, C. von Cube, C. Zimmermann, Ph. W. Courteille, Th. Elsässer, B. Nagorny, and A. Hemmerich, *Phys. Rev. A* **67**, 051802(R) (2003).
 - [8] A. Mosk, S. Jochim, H. Moritz, Th. Elsässer, M. Weidemüller, and R. Grimm, *Opt. Lett.* **26**, 1837 (2001).
 - [9] S. K. Lee, H. S. Lee, J. M. Kim, and D. Cho, *J. Phys. B* **38**, 1381 (2005).
 - [10] H. W. Chan, A. T. Black, and V. Vuletić, *Phys. Rev. Lett.* **90**, 063003 (2003).
 - [11] G. Grynberg and C. Robilliard, *Phys. Rep.* **355**, 335 (2001).
 - [12] M. Greiner, O. Mandel, T. Esslinger, T. W. Hänsch, and I. Bloch, *Nature (London)* **415**, 39 (2002).
 - [13] D. Jaksch, H. -J. Briegel, J. I. Cirac, C. W. Gardiner, and P. Zoller, *Phys. Rev. Lett.* **82**, 1975 (1999).
 - [14] S. Peil, J. V. Porto, B. L. Tolra, J. M. Obrecht, B. E. King, M. Subbotin, S. L. Rolston, and W. D. Phillips, *Phys. Rev. A* **67**, 051603(R) (2003).
 - [15] O. Mandel, M. Greiner, A. Widera, T. Rom, T. W. Hänsch, and I. Bloch, *Phys. Rev. Lett.* **91**, 010407 (2003).
 - [16] R. Drever, J. Hall, F. Kowalski, J. Hough, G. Ford, A. Munley, and H. Ward, *Appl. Phys. B: Photophys. Laser Chem.* **31**, 97 (1983).
 - [17] J. Ye, L.-S. Ma, and J. L. Hall, *J. Opt. Soc. Am. B* **15**, 6 (1998).
 - [18] C. S. Wood, S. C. Bennet, D. Cho, B. P. Masterson, J. L. Roberts, C. E. Tanner, and C. E. Wieman, *Science* **275**, 1759 (1997).
 - [19] C. E. Wieman, M. C. Noecker, B. P. Masterson, and J. Cooper, *Phys. Rev. Lett.* **58**, 1738 (1987).
 - [20] C. S. Wood, Ph.D. thesis, University of Colorado, 1996.
 - [21] Z. T. Lu, K. L. Corwin, M. J. Renn, M. H. Anderson, E. A. Cornell, and C. E. Wieman, *Phys. Rev. Lett.* **77**, 3331 (1996).
 - [22] Z. Kim, S. Y. Kim, S. K. Lee, C. H. Kim, Q-Han Park, and D. Cho, *Rev. Sci. Instrum.* **75**, 2752 (2004).
 - [23] S. K. Lee, B. W. Han, and D. Cho, *Rev. Sci. Instrum.* **76**, 026101 (2005).
 - [24] C. Y. Park, M. S. Jun, and D. Cho, *J. Opt. Soc. Am. B* **16**, 994 (1999).